Journal of Mining and Environment (JME), Vol. 14, No. 4, 2023, 1037-1059

Shahrood University of Technology

Journal of Mining and Environment (JME)

Journal homepage: www.jme.shahroodut.ac.ir

Iranian Society of Mining Engineering (IRSME)

Implementation of Space-Borne Optical Data and Field Investigation for Geo-structural Mapping of an Interior Rift Basin: A Case Study from Kharit Area, Southeastern Desert, Egypt

Ahmed Abdelhalim[1], Eslam Abuelella[2], Shawky Sakran[1], and Said Mohamed Said[1*]

1. Geology Department, Cairo University, Faculty of Science, Giza, Egypt
2. Quality standard information technology, Egypt

Article Info

Received 29 March 2023
Received in Revised form 27 July 2023
Accepted 7 August 2023
Published online 7 August 2023

DOI: 10.22044/jme.2023.12739.2327

Keywords

Geo-structural mapping
Kharit basin
Landsat-8
Rift structure
Cretaceous tectonics

Abstract

Kharit basin is an interior Cretaceous rift basin hosted in a Precambrian basement complex of the Arabian-Nubian shield. Satellite images and potential geophysical data previously outlined the basin without a detailed field study. Kharit area is a remote and hyper-arid area; therefore, the application of remote sensing is essential for completing the process of its geo-structural mapping. A multi-spectral optical dataset of the Landsat-8 and high-resolution images of Google Earth was integrated with the field investigation to classify the lithological units and define structures. That integration between analyzed satellite images and field investigations led to a geological map of a minimum scale of 1:50,000 for the lithological rock units and a maximum scale of up to 1:7000 for the structural mapping. The map shows an elongated NW-oriented rift basin filled by a thick deposit of Cretaceous sequences bounded from the east, west, and south by Proterozoic igneous and metamorphic rocks. Additionally, rift-related volcanic rocks were mapped along the western border fault system of the basin. The main mapped faults were delineated in three trends, NW-SE, WNW-ENE, and N-S, while several folds of NW orientations are developed as a normal drag of the main bounding faults. The Early Cretaceous extension along inherited Precambrian lineaments propagated this fault pattern and its associated folds. These structural elements configured the studied area architecture as several grabens with thick Cretaceous sequences.

1. Introduction

Despite promising opportunities in the Kharit area to explore ores and hydrocarbons, it was geologically neglected for a long time due to its remoteness and hyper-arid climate. Kharit area is about 80 km southeast of Aswan. It is delimited by latitudes 23° 30’ 0” N to 24° 0’ 0” N and longitudes 33° 30’ 0” E to 34° 45’ 0” E (Figure 1). Kharit area extends 200 km-in length and 115 km in width. The area shows NW-SE elongated Mesozoic sedimentary outcrops dissected by a complicated network of wades and tributaries hosted within the Precambrian basement complex [1].

However, the most effective technique to map a remote and vast hard accessibility area is analyzing satellite images. accordingly, there are many authors used the remote sensing technique in the Eastern Desert of Egypt, e.g.[2], [3], [4], [5], [6], [7], [8], [9], [10], [11], [12], and [13]. Occasionally, they utilized a digital color mosaic of Landsat thematic mapper (TM) or the Advanced Spaceborne Thermal Emission and Reflection Radiometer (ASTER) images accompanied with field observations to identify and correlate cross-cutting geologic features on the African and Arabian sides, dominating the Southeastern Desert of Egypt.

Therefore, this area was mapped previously through several regional mapping projects ([14], [15], [16] and [17]. All these maps provided an

Corresponding author: szidan@cu.edu.eg (S.M. Said)

inaccurate conclusive description of the lithology of rocks related to the predominant igneous activity in the area. [4], [18], and [19] concluded that the Kharit area is an elongated NW-oriented Mesozoic sedimentary outlier hosted within the rocks of the Arabian Nubian Shield. A generalized geologic map of Egypt by [14] a 1:4000,000 scale showed a sedimentary cover of the Nubia sandstone complex and undifferentiated Cretaceous sediments. Similarly, a regional geological map of [15] mapped the sedimentary units in the study area as undifferentiated Cretaceous sediments overlain by Quaternary deposits. According to the [16] geologic map at scale 1:500,000, the studied area is occupied by Late Cenomanian to Early Campanian clastic and Quaternary aeolian and alluvial deposits. However ,neither the previous works nor the geologic maps report a detailed structural framework of the Kharit area.

Therefore, geo-structural mapping is essential to provide basic geological and structural knowledge for further geological studies and natural resource explorations. However, the hyper-arid climatic conditions without vegetation cover characterized the Kharit area causes favor conditions to apply optical remote sensing technologies for geological mapping. Additionally, extensive field trips validated the interpretation and analyses of the satellite images, increasing the accuracy of the produced map.

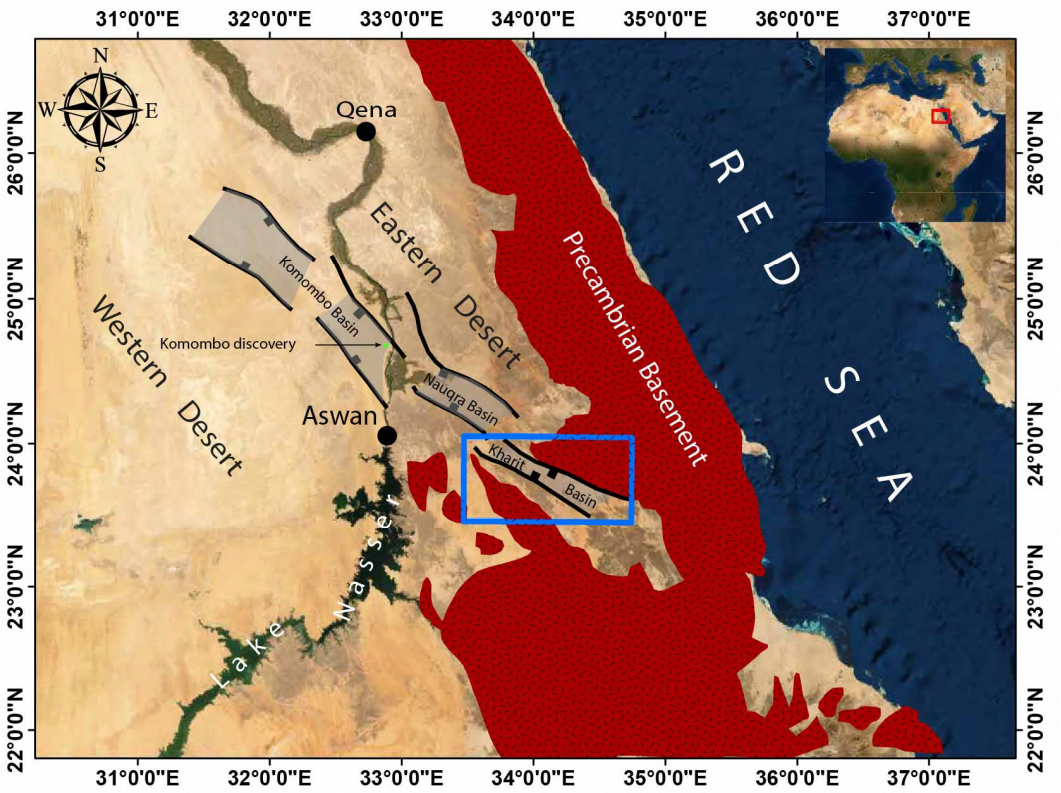

Figure 1. Location map of southern Egypt basins and the area of the present study (blue rectangle). Faulting and basin geometry is after [20]. The Precambrian basement complex in the Eastern Desert of Egypt is after the Geological map of Egypt (1987). The image in the background is the Digital Globe, GeoEye, Earthstar Geographics, CNES/Airbus DS, USDA, USGS, Aero GRID, IGN, and the GIS User Community.

2. Geological Setting

The surface geological setup of southern Egypt is dominated by exposures of the Neoproterozoic (900–550 Ma) basement of the Arabian Nubian Shield dissected by intracratonic rift basins. The basement complex of the Arabian Nubian Shield is a result of the Pan-African orogeny [21], [22]. This orogeny is sub-divided into three major evolutionary stages: (a) the accretion stage occurred between 870–670 Ma; (b) the collision stage lasted from 650 Ma to 640 Ma, and (c) extensional collapse initiated directly after the termination of the collision [23]. Studied the structural synthesis of theArabian Nubian Shield at a regional scale. They described the orientation

of structures south of Wadi Kharit-Wadi Hodein mainly alternating between E-W and N-S and that the orientation of structures northward from Wadi Kharit-Wadi Hodein is NW- SE [24].

A sedimentary basin system consisting of Kharit, Nuqra, and Komombo occupies a vast area of southern Egypt. Two commercial discoveries are recorded in the Komombo basin west of the Nile River. The eastern part of this basin system, occupied by the Kharit and Nuqra basins, must be better explored [25]. This basin system is a NW to NNW oriented Early Cretaceous intracratonic rift basin in southern Egypt [20], [26] and bounded and dissected by several E-W oriented strike-slip faults [27], [28], [29], and [30].

Kharit basin is the southern segment of the South Egypt rift system and appears as an elongated NW-oriented sedimentary inliers within crystalline basement rocks of the Arabian -Nubian shield. Rock succession of the study area consists of two sequences: the igneous and metamorphic rocks of the Precambrian and the Phanerozoic sediments and volcanic rocks (Figure 2).

The surface sequence of the study area is subdivided into three main stratigraphic units [16]. The oldest unit is the Abu Aggag formation which crops out in the southwestern and northeastern parts of the Kharit area. The Upper Cretaceous Timsah and Umm Barmil formations overlie Abu Aggag Formation (undifferentiated Cretaceous). The Quaternary deposits of wadis, alluvial fans, and dunes overlie the latter formations. According to the drilling result by Repsol 1998, Centurion and Trasnglobe 2007; the subsurface of the Kharit basin is dominated by the Lower Cretaceous clastic (Kommbo and Six Hills formations) (Figure 2).

3. Materials and Methods

Landsat 8 (OLI/TIRS scene) was launched in 2013 as the latest satellite in a Landsat program that provides a unique 45-year data record of the Earth's land surface. Landsats 1, 2, and 3 were launched in 1972, 1975 and 1978, respectively. Landsat 4 was launched with the MSS, and a new instrument called the Thematic Mapper (TM). Landsat 5, a duplicate of Landsat 4, was launched in 1984 and returned scientifically viable data for 28 years - 23 years beyond its 5-year design life. Landsat 6, equipped with an additional 15-meter panchromatic band, was lost immediately after launch in 1993. Finally, Landsat 7 was launched in 1999 and performed nominally until its scan line corrector (SLC) failed in May 2003.

The mapping technique was based on integrating remote sensing datasets and field observations. The pre-processing and the processing of Landsat-8 images were performed with Envi 5.3. The geological map and visual interpretation of structural elements were produced with ArcGIS 10.4. The geo-referencing of notes and images during the field trip was achieved by UTM Geomap mobile application. The remote sensing datasets are a multispectral optical dataset of the Landsat-8 scenes and high-resolution images of Google Earth. Landsat-8 scenes were accessible on the United States Geological Survey (USGS) archives. The area is covered by three scenes acquired in February 2018 with Universal Transverse Mercator (UTM) projection, zone 36 N, and World Geodetic System 1984 (WGS-84) datum with a path and row map index; P173R44, P174R43, and P174R44 (Figure 3a). While high-resolution images of Google Earth are roughly 65cm pan-sharpened (65 cm panchromatic at nadir, 2.62 m multi-spectral at nadir). The processing started with Radiometric Calibration, then the Fast Line-of-sight Atmospheric Analysis of Spectral Hypercubes (FLAASH) [31], [32], [33], [5], [8], [10]. These steps were followed by Reflectance scaling to correct the resulting negative value from Fast Line-of-sight Atmospheric Analysis of Spectral Hypercubes (FLAASH) correction [34]. The processes end with the Gram-Schmidt image pan sharpening to enhance the spatial resolution of multispectral bands [35] (Figure 3b). Image analysis relied on supervised classification with training pixels that were used to define the lithological classes in the study area. Training pixels discriminated on specific false-color composite (FCC) images and images resulting from the decorrelation stretch (DS).

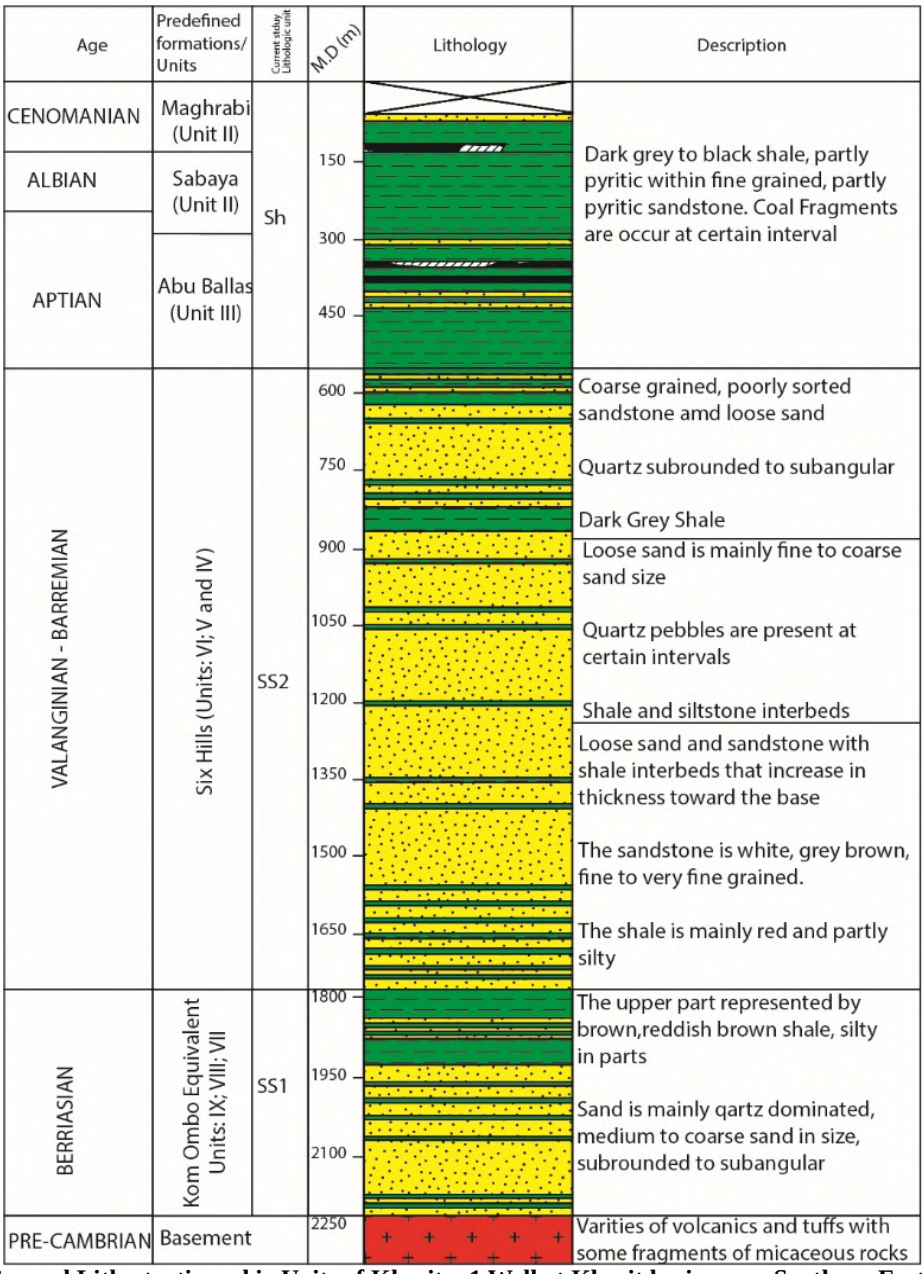

Figure 1. General Lithostratigraphic Units of Kharit – 1 Well at Kharit basin area, Southern Eastern Desert, Egypt modified after (Repsol, 1998; Centurion and Transglobe, 2007).

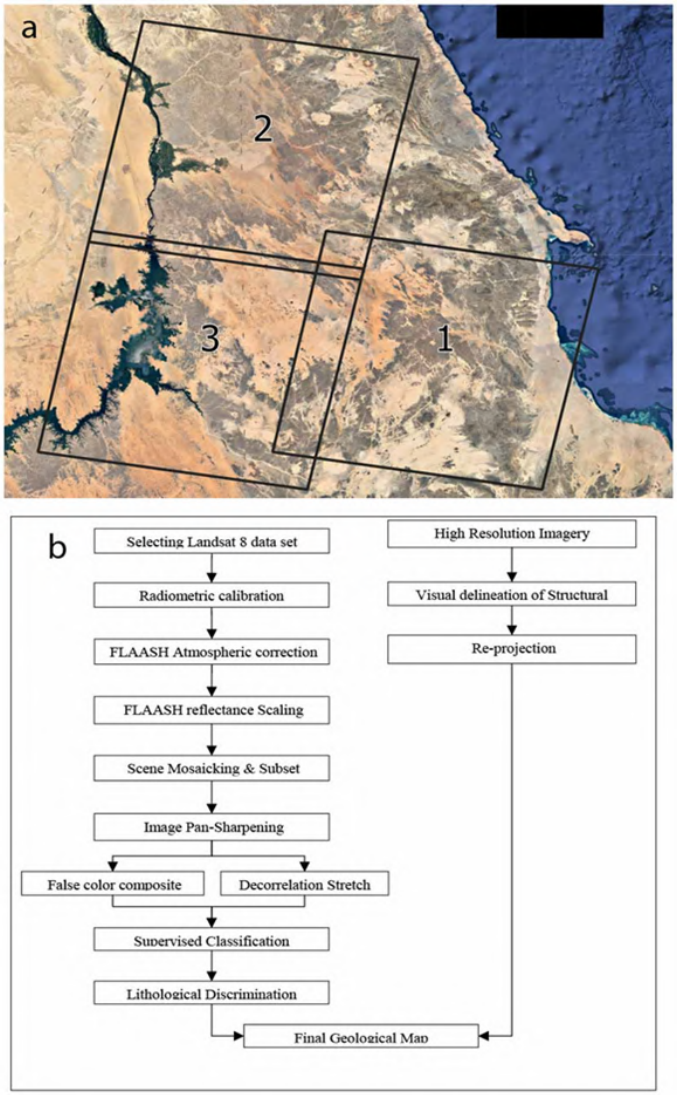

Figure 2. a) Illustrates three scenes acquired in February 2018, with the following path and row map index (P173R44, P174R43, and P174R44).

- **Scene 1: P173 R44 2018 / 02 / 17 LC81730442018048LGN00**
- **Scene 2: P174 R43 2018 / 02 / 08 LC81740432018039LGN00**
- **Scene 3: P174 P44 2018 / 02 / 08 LC81740442018039LGN00**

b) The flowchart of the primary spatial analysis and geo-processing steps applied to different remote sensing datasets in the present study.

The supervised classification training pixels of the different rock units covering the study area were carefully discriminated using false color composite images (FCC) of (6,3,2) and (7,5,3) multi-spectral bands combination in red-green-blue order (Figure 4). The selected bands for false-color composite (FCC) were chosen since they showed the most evident contrast between the geological units as documented by various resources [36], [37], [38], [6],[7],[39]

Decorrelation stretch (DS) [40] reduces the correlation between multispectral bands and generates more distinctive and saturated colors. Decorrelation stretch was applied on 7, 5, 3, and the 6, 3, and 2 false-color composites (FCC) to ensure an accurate selection of training pixels used in supervised classification (Figure 5).

The supervised classification generates an image showing the different rock units in the study area. In supervised classification, representative sample information clusters on the raster dataset for the area of interest [41] are selected. Usually, for geological mapping, the selection of the sampling sites requires prior integration between previous geologic maps and images produced from image processing

techniques. Since the reflectance / thermal of the same rock unit changes due to the irregular effects of weathering, deposition, and diagenesis [42] the maximum likelihood supervised classification algorithm was used (Figure 6*)*.

The automatic detection of linear features needs to be improved for structural mapping in the study area. Therefore, geological structural features were identified by visually interpreting high-resolution images (Google Earth). Geological structures were visually interpreted by recognizing the differences between any or all elements of visual interpretation (tone, shape, size, pattern, texture, shadow, and association) introduced by [43] in combination with previously identified geological units (Figure 7).

In a validation step, a field trip was carried out during March 2019 in the northern parts of the study area between latitudes 23°49'44.57" & 23°57'59.75" and longitude 34°01'50.85" & 33°29'06.58" (Figure 8). The validation area was about 830 km^2 and was studied through 35 field stations which were selected carefully via remote sensing techniques (Figure 8). Geological outcrops were sampled to validate supervised classification input representative sampling sites of the lithological units. The dip and strike of the different structural elements and rock units on the mapped faults' hanging and foot walls were measured. Finally, three geological cross-sections were constructed to demonstrate the structural geometry of the mapped area.

4. Results

4.1. Lithology

The area of study is dominated by Quaternary deposits represented by dunes in the southernmost part, which appear as light grades of yellow colors and buffy orange on false-color composite (FCC) (7, 5, 3) and false-color composite (FCC) (6, 3, 2), respectively. Visually recognizable bodies with multi-colored (rock fragments) represent wades and alluvial fans. The study area includes three sedimentary rock units; a shale unit (Sh); a ferruginous sandstone unit (SS2), and a brownish kaolinitic sandstone unit (SS1). These units appear on false-color composite (FCC) (6, 3, 2) as brownish orange, greenish grey, and reddish-brown, respectively. On false-color composite (FCC) (7, 5, 3) shale unit (Sh) is shown as tannish yellow; the ferruginous sandstone unit (SS2) is shown as greenish-grey and brownish kaolinitic sandstone unit (SS1) is shown as pale brown (Figure 4). Syenitic ring complexes. Trachytic-basaltic dykes are also recorded in the study area. These rocks occur in specific localities and appear as dark grey rocks on false-color composite (FCC) (7, 5, 3) and false-color composite (FCC) (6, 3, 2) (Figure 4).

Basement rocks in the study area are distinguishable from each other. On false-color composite (FCC) (6, 3, 2) (G1), weathered granitic rocks appear as a flush rose (Figure 4), while it appears as pale beige on false-color composite (FCC) (7, 5, 3) (Figure 4). On false-color composite (FCC) (6, 3, 2) weathered diorite rocks appear as bluish grey (Figure 4), while it appears as pale greyish purple on false-color composite (FCC) (7, 5, 3) (Figure 4). Although the gabbroic rocks are restricted to a small area in the northern part of the study area, it is distinguished as dark greenish-blue rocks on false-color composite (FCC) (7, 5, 3) and false-color composite (FCC) (6, 3, 2) (Figure 4). On false-color composite (FCC) (7, 5, 3) metasediments are shown in shades of purple color, similarly, metasediments on false-color composite (FCC) (6, 3, 2) are shown in shades of a greyish white. In false-color composite (FCC) (6, 3, 2), ophiolitic metagabbro is greyish black, while serpentinite is teal blue.

There are some rocks appear in similar colors on the preselected false-color composite (FCC), for example, the brownish kaolinitic sandstone unit (SS1) and intrusive metagabbro to meta diorite (Mgi) are displayed in different grades of brown-colored rock. Thus the decorrelation stretches utilized (DS) (6, 3, 2) effectively to solve the ambiguity that appears on the false-color composite (FCC) (7, 5, 3) and false-color composite (FCC) (6, 3, 2) with unique colors for similarly colored rocks, where the contrast between the brownish kaolinitic sandstone unit (SS1) and intrusive meta gabbro to meta diorite (Mgi) is established, as they appear as purple rocks and greenish rocks, respectively (Figure 5). Another segregation is obtained by decorrelation stretch (DS) (7, 5, 3) between syenitic ring complexes and trachytic-basaltic intrusions (Rc) and ophiolitic metagabbro (Mgo), which both appear on false-color composite (FCC) (7, 5, 3) and false-color composite (FCC) (6, 3, 2) as dark grades of grey rocks, while syenitic ring complexes and trachytic-basaltic intrusions (Rc) appears as green leaf rocks, and ophiolitic metagabbro (Mgo) appears as greyish-red rocks (Figure 5).

The field verification for all previously mentioned results from the interpretation of remote sensing datasets confirms that the

Mesozoic cover in the study area consists of three major sedimentary units. The oldest unit unconformably overlies the Precambrian metasediments to the east and is followed westwards by the overlying younger sedimentary units (Figures 6 & 9). Brownish-colored pebbly sandstone unconformably overlies the basement rocks on the western side of the study area. This unit's exposure localities, stratigraphic order, and lithological description strongly agree with the predefined brownish kaolinitic sandstone (SS1) sedimentary unit solid mapped through the Landsat-8 image. Finally, an overlying unit is described as a multicolored fine to medium-grained ferruginous sandstone (Figures 9 d & f). This unit is exposed at certain narrow uplifted blocks along the Aswan-Halaib highway and overlies the brownish kaolinitic sandstone unit (SS1). Various fine clastic associations occur on the low relief exposures along the Aswan-Halaib highway. These clastics are recorded as alternating intervals, green shale, black shale, shale with plant remains, and tiny inter-beds sandstone (Figure 9e). The nepheline syenites and the associated rocks are validated and confirmed (Figures 9b & c). The basement complex bounding the study area comprises various granitic rocks and pelitic schists.

4.2. Structural architecture

Kharit basin is a sedimentary outlier surrounded by Precambrian rocks from East, West, and South. Two subparallel boundary fault zones of the Kharit basin are formed mainly from NW-SE oriented faults linked together through N-S faults. The northeastern boundary fault zones throw toward the southwest. In contrast, the southwestern fault zone throws toward the northeast, which causes subsidence that provides accommodation space and allows the accumulation of the existing sedimentary units. Other faults belonging to the NW-SE fault set are the main controller of the distribution of sedimentary units. The continuity of the E-W fault cut through the northeastern basement rocks. Various fault sets predominantly represent the structural features in the study area, whereas folds are the following features. The structural measurements through the selected field stations indicate that the general dipping of the Mesozoic rocks through the study area ranges between 7° up to 20° in the northeast direction. At the same time, this dip changes in certain localities due to faulting and folding effects. For example, two folds exist near the Aswan-Halaib highway with fold axes trending NW-SE and NE-SW. In addition, NW plunging synclines and anticlines are mapped in the study area (Figure 7).

Four fault sets occur in the studied area with the arrangement in descending order of frequency as NW-SE, WNW-ESE, E-W, and N-S striking faults (Figure 10).

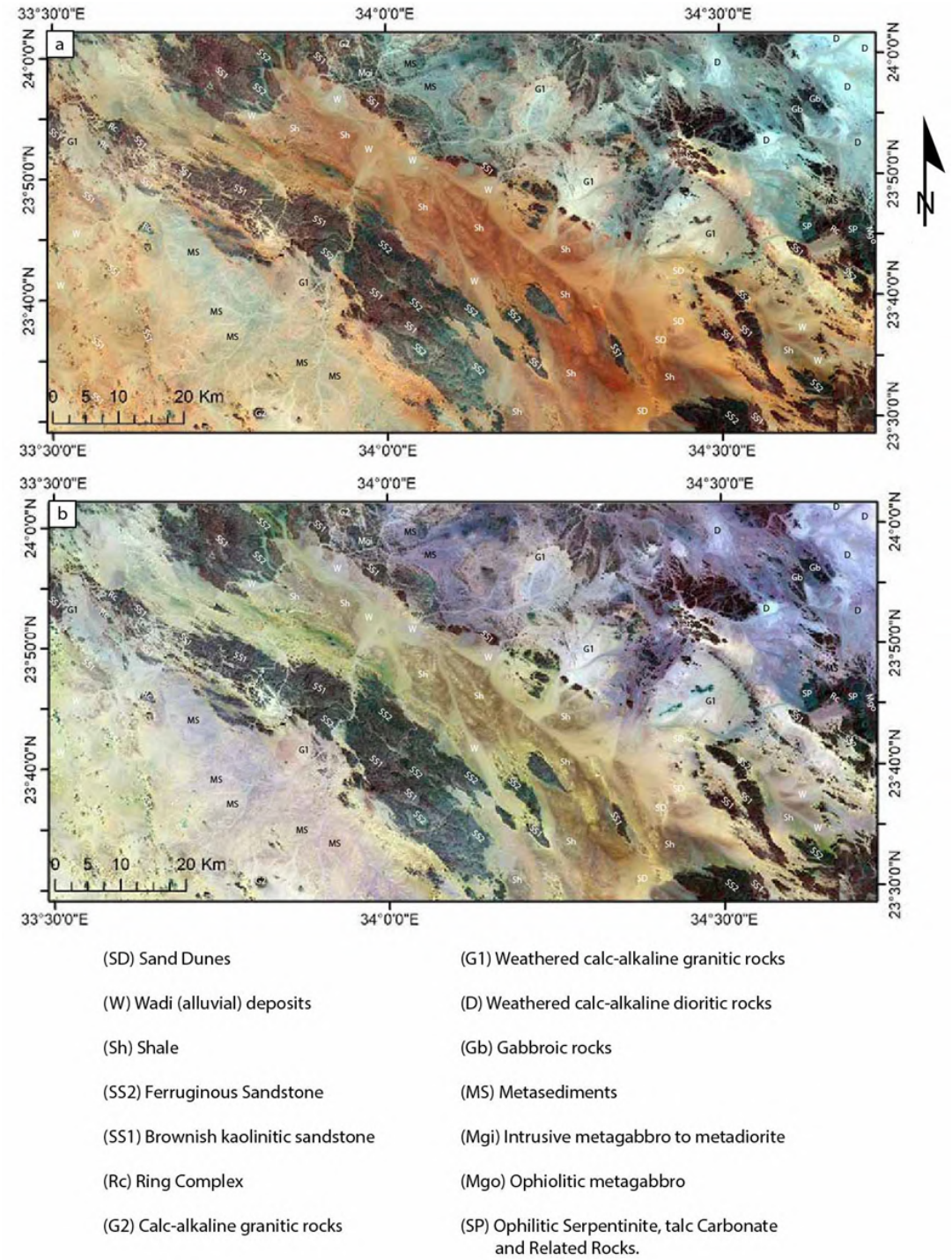

Figure 3. Illustrates false-color composite (FCC) of Landsat 8 image used to differentiate various lithological units (a) Bands 6, 3, 2 in RGB order, respectively. (b) Bands 7,5 and 3 are in RGB order, respectively.

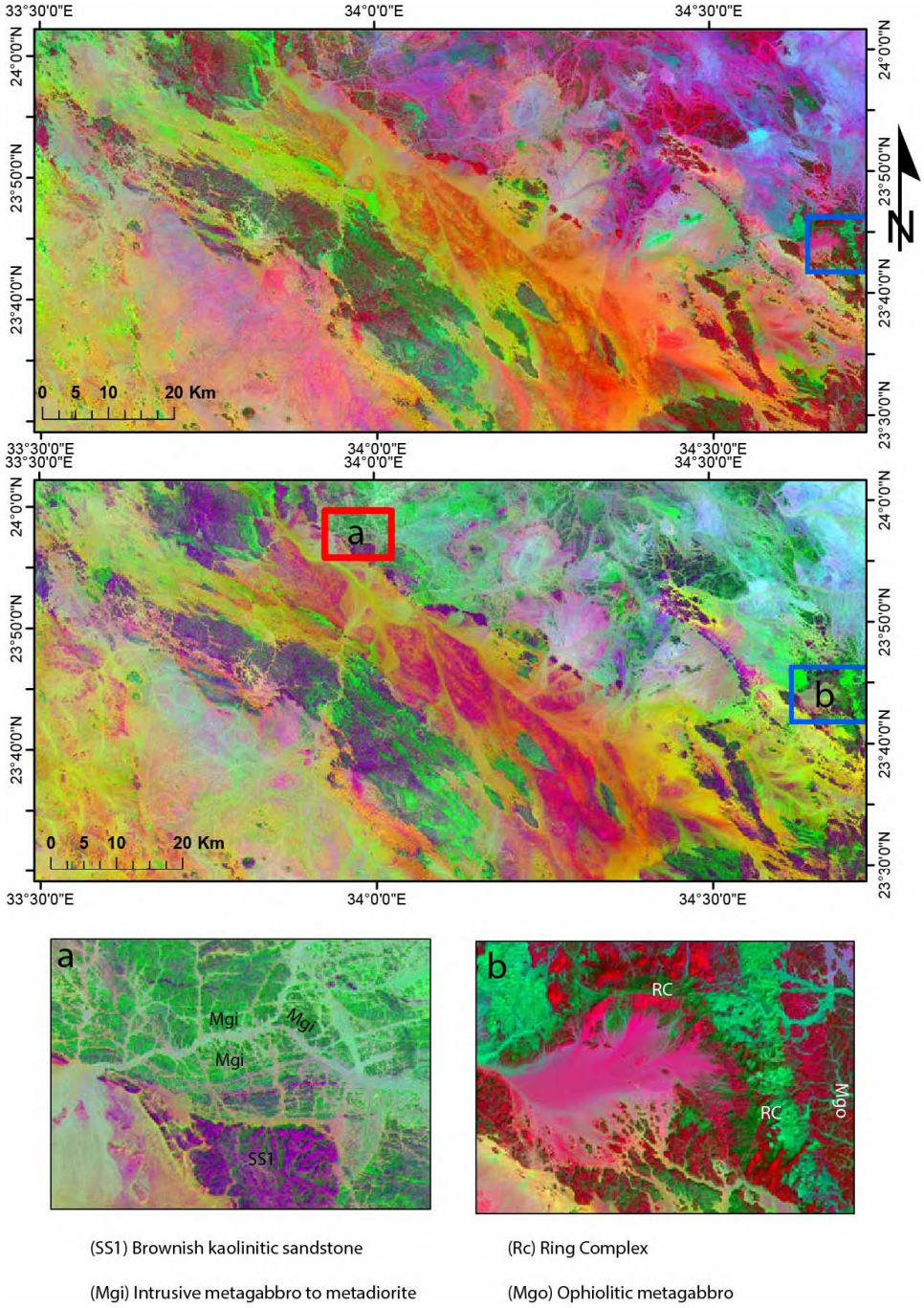

Figure 4. (a) Demonstrates decorrelation stretch (DS) of Landsat 8 image of 6,3and two bands in RGB order used to differentiate between rocks related to ring complex and Ophiolitic metagabbro. (b) Elucidates decorrelation stretch (DS) of Landsat 8 image of 7, 5, 3 bands in RGB order used to differentiate between brownish kaolinitic sandstone and intrusive metagabbro -metadiorite.

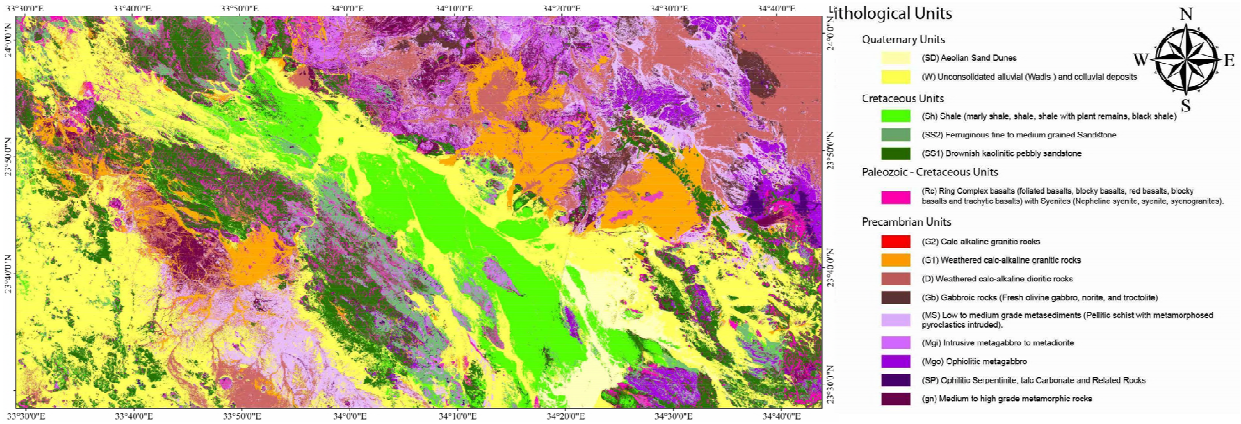

Figure 5. Illustrates the initial lithological classes that ensued from supervised classification results applied to Landsat images of the Kharit basin.

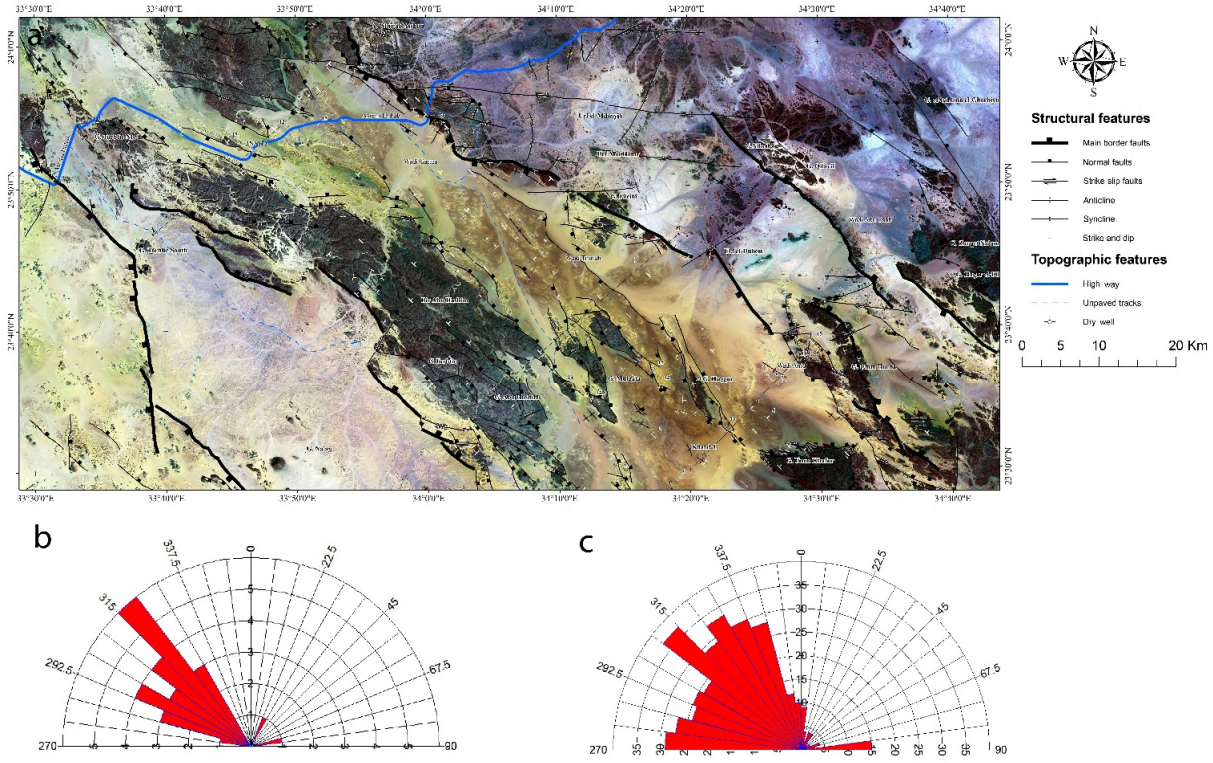

Figure 7. (a) False-color composite (FCC) of Landsat 8 image (7, 5, and 3 bands in RGB order) illustrates the various surface structural features in the study area. (b) The Rose diagram of folds formed in the Kharit basin shows that most folds formed in the study area are in NW alignment. (c) Rose diagram of faults affected Kharit basin showing that most faults affected the study area strike in north-west direction.

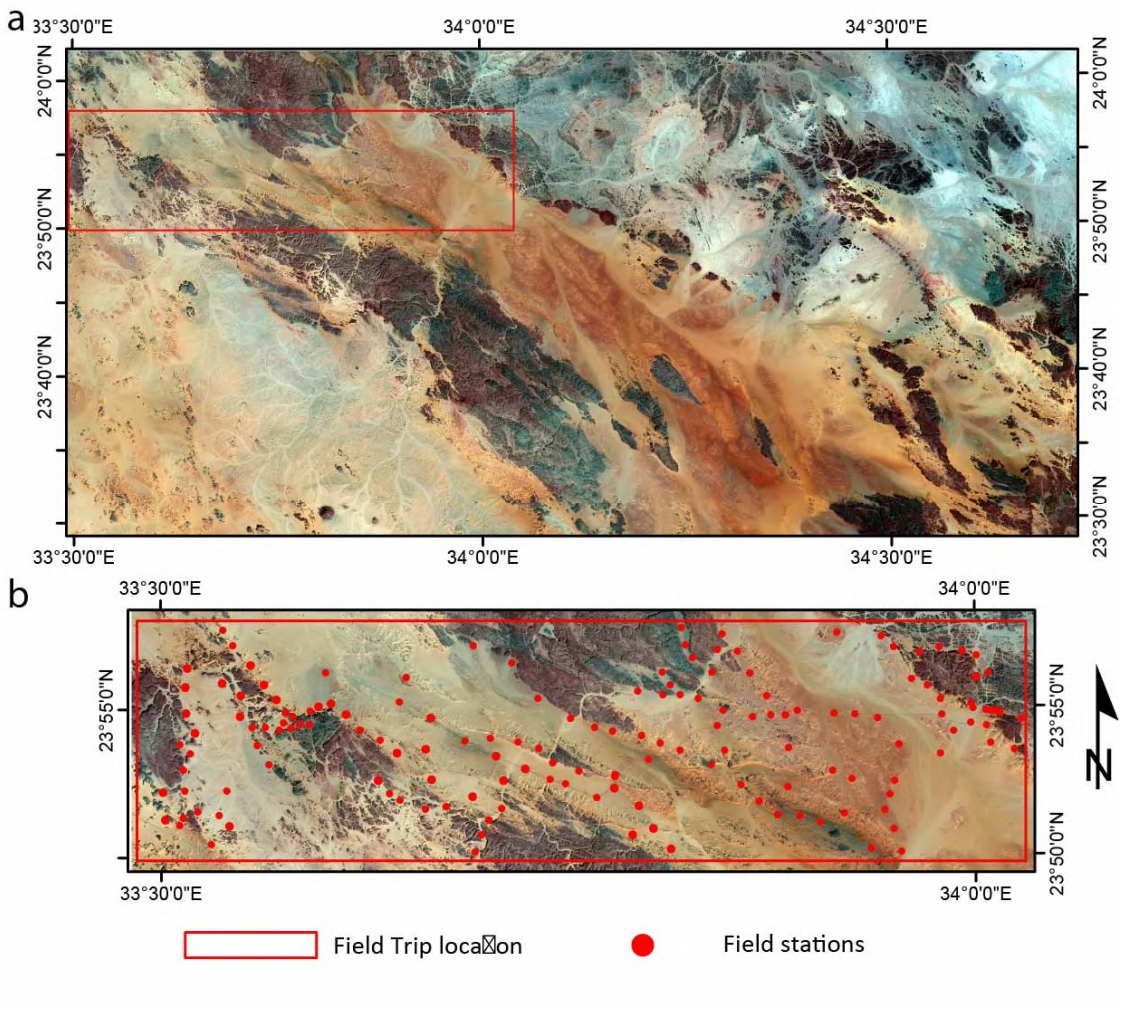

Figure 8. (a) Illustrates observation stations of the field trip illustrated on the false-color composite (FCC) of Landsat 8 image (bands, 6, 3, 2 in RGB order). (b) The field station was used for structural measurements and lithological sampling.

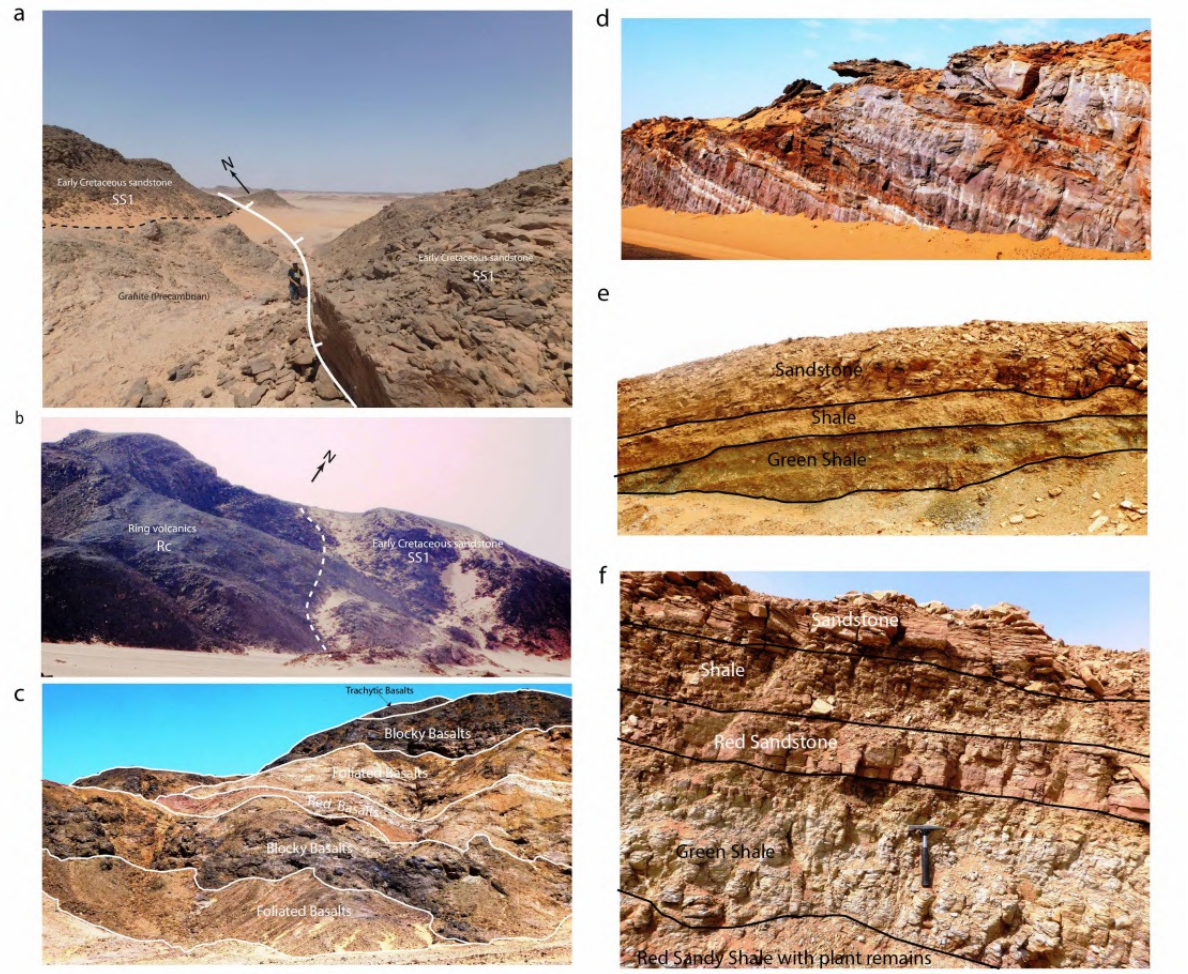

Figure 6. Field photos show (a) N-S normal fault juxtaposes SS1 (brownish kaolinitic pebbly sandstone) against Precambrian basement rocks (granites). (b) The igneous rocks of the Tarbtie North ring complex are overlain by SS1 (brownish kaolinitic pebbly sandstone). (c) Extrusive Tarbtie North ring complex rocks consist of several zones of basalts (foliated basalts, blocky basalts, red basalts, blocky basalts, and trachytic basalts). (d) Fine to medium-grained sandstone with reddish pigment due to iron ore enrichment. (e & f) Marly shale, green shale, and shale with plant remains of the main shale unit in the studied area.

The NW-SE fault set is the predominant fault set in the studied area. This set of faults shows normal dip-slip movements. NW-SE fault set affects all exposed rock units. The number of NW-SE faults increases eastward through the study area. The NW-SE fault set includes the main structural elements that control the lithological units' distribution and define the Kharit basin's shape *(*Figure 7). The longest and most important interpreted faults are the rift border faults at both sides of the rift. The Eastern rift border fault system consists of several segments of NW-SE orientation linked by short WNW-oriented faults. On the other hand, the western border fault system involves linked segments of NW-SE and N-S orientation (Figures 7 & 10). The border faults juxtapose the basement complex to the east and the west against brownish kaolinitic sandstone (SS1) in the basin direction (Figures 7 & 10).

E-W to WNW oriented faults extends for distance long-distance cut through the rift border faults. This set of faults shows dextral strike-slip movement. They are predominant in the eastern part of the study area (Figure 7). To the north of Wadi Garara, the WNW fault dextrally offsets NW-SE faults, N-S faults (Figures 7 & 10).

The N-S fault set shows normal left-lateral movements. This fault set is inherited from Precambrian and reactivated as a part of the rift border fault and internal fault system during the Cretaceous extension. This set's most obvious apparent faults are the faults bounding the western side of the southwestern shoulder of the basin. These faults juxtapose the basement complex to

the east with the brownish kaolinitic sandstone unit (SS1) to the west (Figures 7 & 10).

Most mapped folds in the study area have a NW-SE orientation. Therefore, the NW-oriented synclines are developed as a normal drag in the downthrown side of the main rift-related faults (Figure 10). Few NE-oriented folds are mapped at the intersection of NW and WNW-oriented faults (Figure 10). All the mapped folds were developed as drag along the corresponding fault.

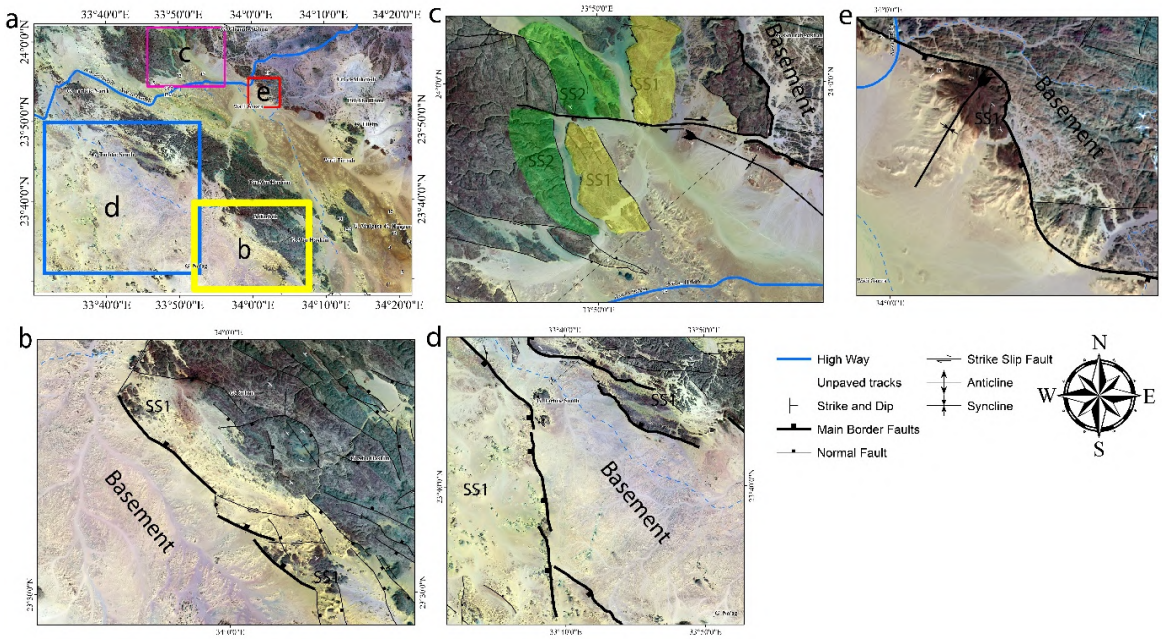

Figure 10. False-color composite (FCC) of Landsat 8 image (7, 5, and 3 bands in RGB order) used to illustrate (a) location map for the selected set of examples. (b) The fault zone bound the basin to the southwest; these faults strike NW-SE and down-throw to the northeast, which affected the Cretaceous sedimentary succession accompanied by NW oriented forced folds. (c) E-W dextral strike-slip fault offsets other fault sets and lithological units. This fault links the NW-SE and N-S faults of the fault zone bound by the basin to the northeast. In addition, a significant synclinal folding effect appears. (d) A horst block of basement rocks forming the southwestern basin shoulder, this horst block is bounded to the southwest and northeast by fault zones of N-S and NW-SE faults, respectively. (e) A fault zone bounds the eastern side of the Kharit basin; this fault zone is formed by the link between N-S and NW-SE fault sets.

The geological relationship between identified structural features and mapped lithological units is best viewed on the geological cross-section and seismic reflection profiles. Hence, three geological cross-sections (Figure 11b) are established, and three seismic sections were interpreted (Figures12 & 13 & 14) to cover the different parts of the studied area. A-A' cross-section that simulates the structural configuration at the northern parts of the study area. The A-A' shows that two basement shoulders border the study area to the northeast and southwest. Two major multi-segmented fault zones with strike-oriented NW-SE juxtapose the basement shoulders to the brownish kaolinitic sandstone unit (SS1) and the northeastern segments of these bounding faults down-throw to the southwest. In contrast, the southwestern segments of these bounding faults down-throw to the northeast. These subparallel fault zones bounding the study area cause significant subsidence of interlaying strata to form major graben. This major graben is subdivided into three smaller sub-grabens; uplifted areas with narrow extensions separate these sub-grabens. B-B' cross-section constructs the structural configuration of the middle part of the area. This cross-section paths through several highly daunted sedimentary units of G. Abu Hasheem and G, Mulgata in the southwest to reach the low topographic area of Wadi Timsah in the northeast. In this cross-section, several tilted fault blocks were recognised; the deepest blocks are the northeastern ones. C-C' cross-section traverses the southernmost part of the study area. Two graben blocks are separated by crucial horst block, which can describe the structural configuration of this part of the studied area. This cross-section has exceptional credibility as Kharit-

1 well penetrates one of the defined graben blocks (Figure 11A). The oldest sedimentary unit (brownish kaolinitic sandstone) is juxtaposed against metasediments or weathered granitic rocks to the northeast and southwest through various sets of faults with strike NW-SE, and E-W oriented faults. The internal rift faults of a NW-SE orientation juxtapose younger ferruginous sandstone (SS2) against a brownish kaolinitic sandstone unit (SS1), causing shallow burial of underlying brownish kaolinitic sandstone unit (SS1). Following that, a deeper burial of brownish kaolinitic sandstone unit (SS1) and ferruginous sandstone unit (SS2) along NW-SE faults. The rift interior NW –SE oriented faults dip due NE and SW forming small sub-basins of grabens and half grabens (Figure 11A). Accommodation horsts separate these sub-grabens.

Seismic sections show the chart basin's configuration, exhibiting geometrical variation along and across its axis (Figures 12 and 13). Along the NW-SE seismic profile, the Kharit basin encompasses two sub-basins formed by several normal faults. The two sub-basins are separated by broad intra-basinal horst in the central part of the study area. The Northern sub-basin is poorly understood due to the lack of NE-SW seismic profiles perpendicular to the rift-related structures. The Southern sub-basin shows strata dipping to the southeast.

The first NE-SW (Line 2) seismic profile shows the northern sub-basins configuration. The northern sub-basin is configured as a tilted fault block toward the northeast. Fault (F12) is the eastern boundary fault down throw to the northwest. While fault (F14) is the western boundary fault down throw to the northeast. Multiple synthetics (F9, F15, F13) configured the tilted fault blocks as half grabens.

The second NE-SW seismic profile (Line 2) shows the configuration of southern sub-basins encompassing two sub-grabens (depocenters) (Figure 14). The northeast boundary fault system (F1) subsided the eastern sub-graben (depocenter). Two NW-SE faults bound the western Sub-graben. The northeast boundary fault system (F4) is down to the southwest, while the southwestern boundary fault system (F16) is down to the northeast. Each major graben is further subdivided into several intrabasinal troughs and highs bounded by synthetic dip-slip normal faults and antithetic dip-slip normal faults (F16, F7, F143, F5, F4, F23).

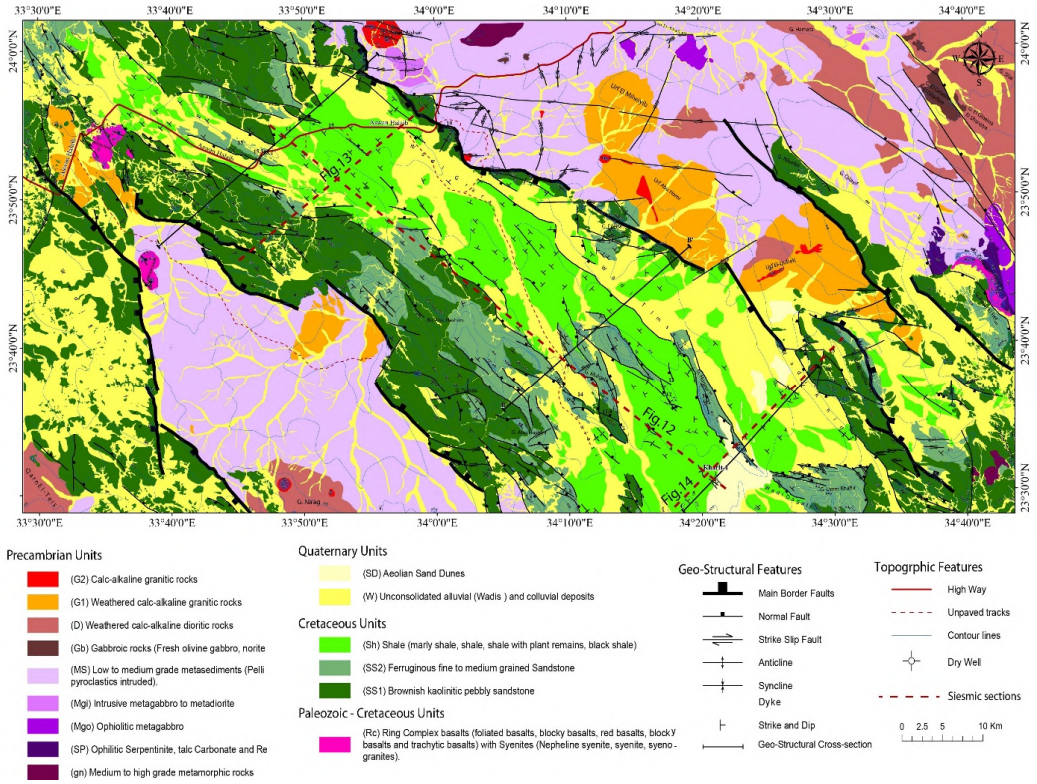

Figure 7A. Illustrates the final layout of the Geo-Structural Map of Kharit Basin, southern Eastern Desert, Egypt, at scale 1:50,000 show the final map produced by combining lithological units, interpreted structural elements, and topographic elements and includes an index map showing the geographic location of the studied area.

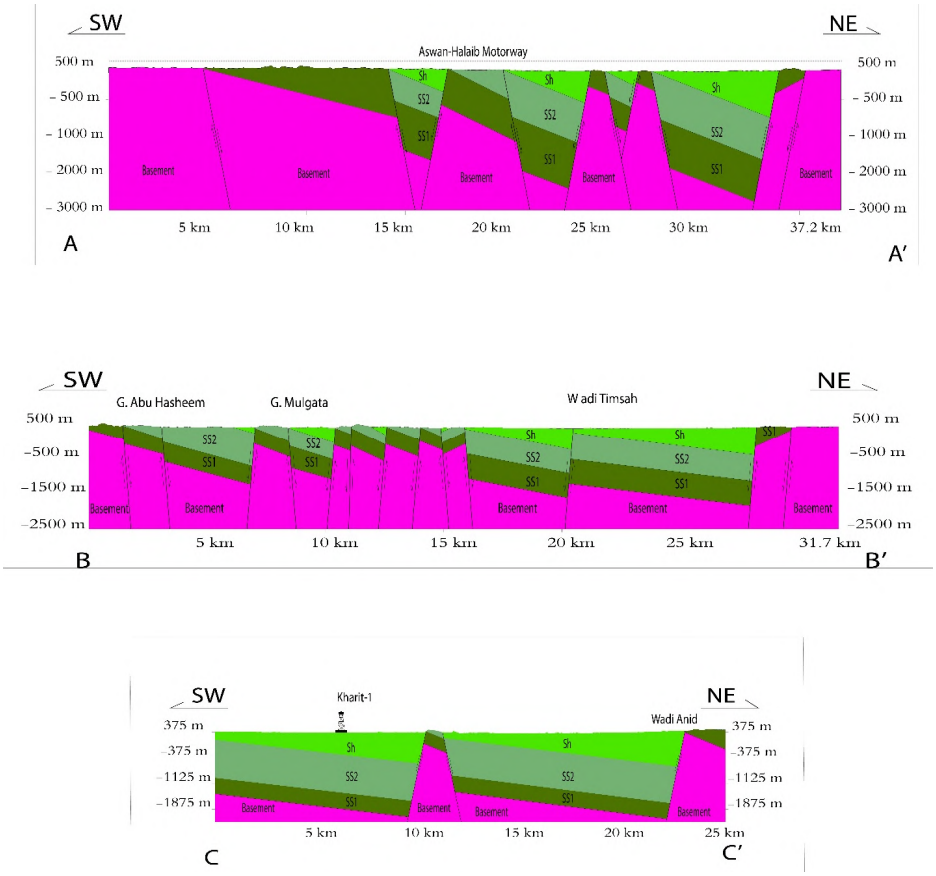

Figure 11 B. The three representative geo-structural cross-sections of Kharit basin A-A', B-B', and C-C' at vertical exaggeration = 2.5.

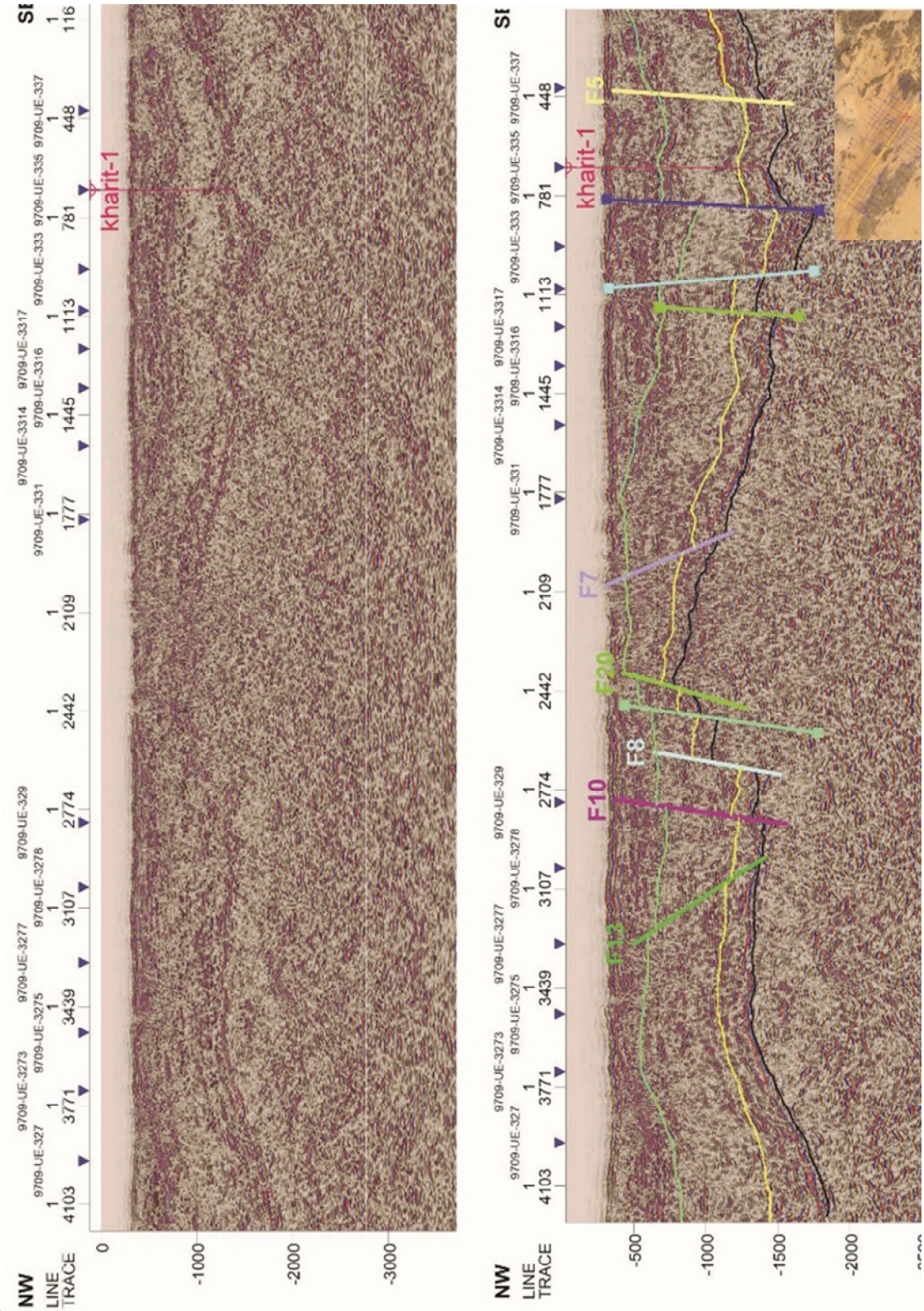

Figure 8. Interpreted 2D-Seismic Line (along the elongated axis of the basin) shows two sub-basins separated by intrabasinal high. Black line represents top Precambrian Basement, yellow line represents top Komombo Shale, green line represents top six Hill Formation.

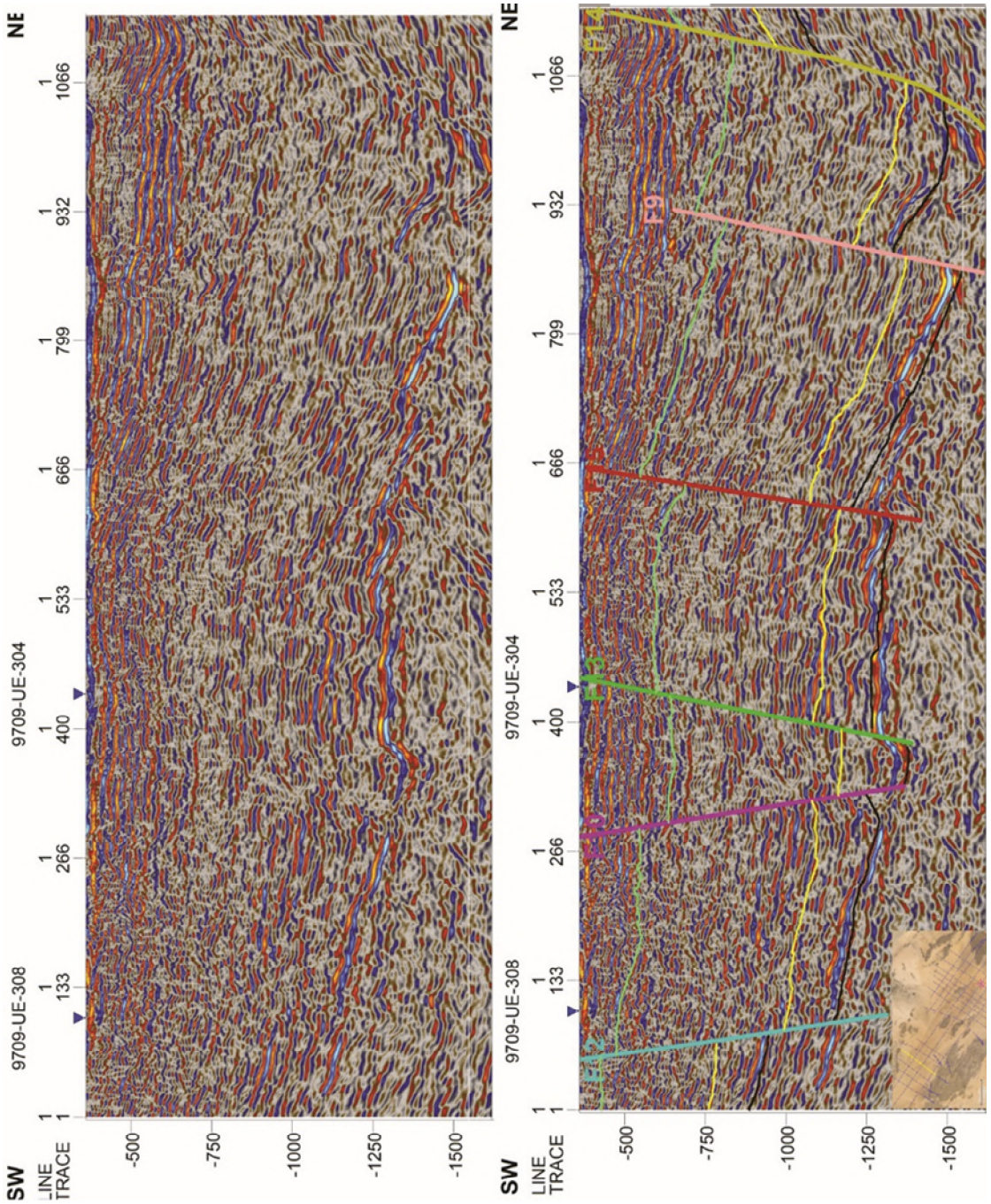

Figure 9. Interpreted 2D-Seismic of NE-SW orientation shows the structural configuration of the northern sub-basin. Black line represents top Precambrian Basement, yellow line represents top Komombo Shale, green line represents top six Hill Formation.

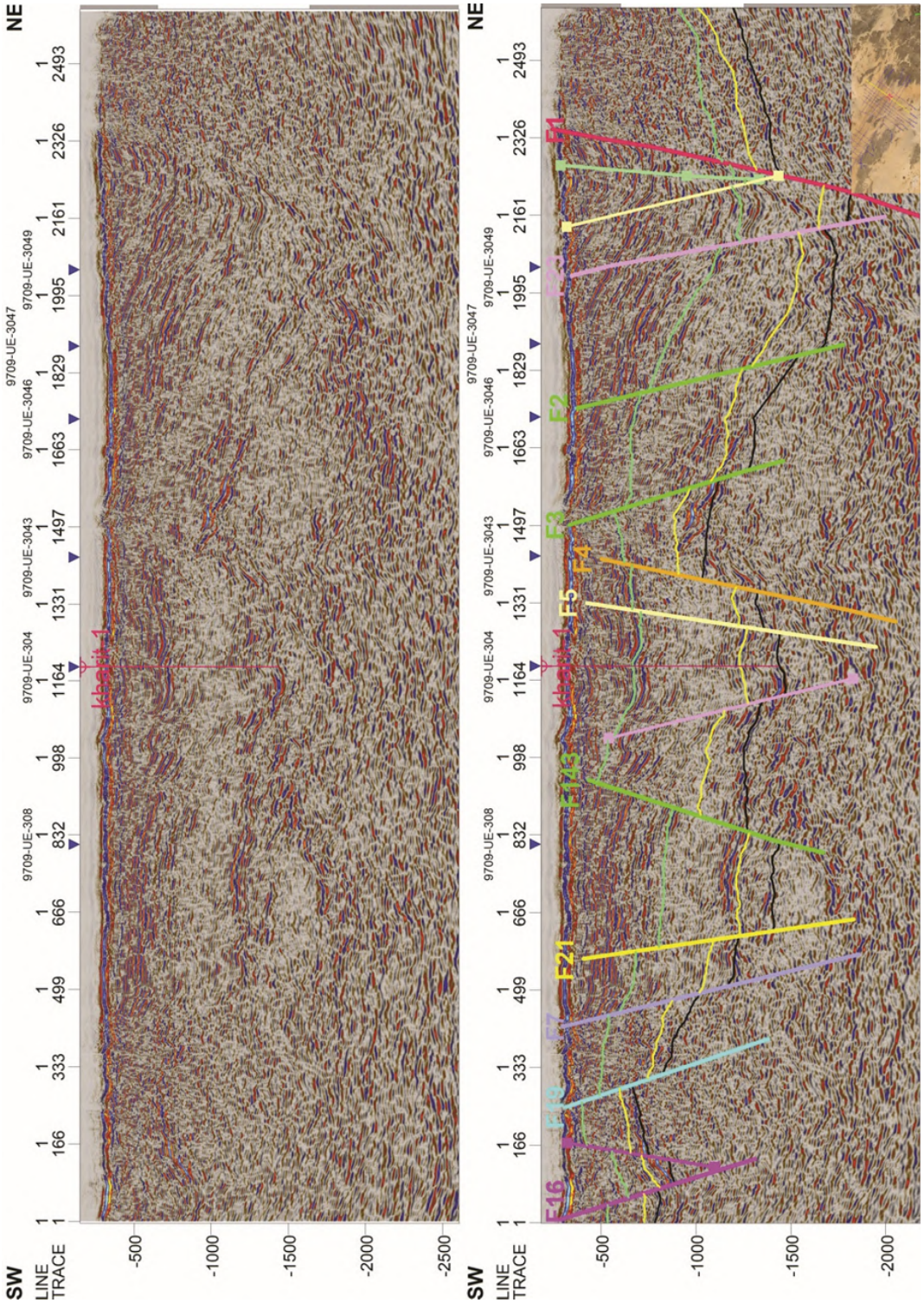

Figure 10. Interpreted 2D-Seismic of NE-SW orientation shows the structural configuration of the southern sub-basin. Black line represents top Precambrian Basement, yellow line represents top Komombo Shale, green line represents top six Hill Formation.

5. Discussion

The current geo-structural map provides new modifications and updates in the distribution and type of the lithological units as well as the structural architecture of the Kharit basin. This map has a minimum scale of 1:50,000 for lithological mapping and a maximum scale of up to 1:7000 for structural mapping. In addition, the produced map includes elevation contour lines to define the topographic nature of the study area and structural measurements of dip and strike of the different planar structural elements.

Considered that all sedimentary rocks covering the study area belong to the Nubia Formation coeval Upper Cretaceous marine beds composed of variable classics [15]. The Quaternary wadi and playa deposits were illustrated as irregular bodies overlain preceding geological units. It also roughly defined ring complexes in the study area as semicircular or semi-elliptical units composed chiefly of alkaline syenites. These ring complexes were dated as younger than Cretaceous sediments. Integrating remote sensing and field observations enabled the definition of three sedimentary units (brownish kaolinitic sandstone unit, ferruginous sandstone unit and shale unit). The visual interpretation of all available remote sensing datasets allowed detailed identification of wadis in the studied area and the detection of dunes in the southern part of the studied area (Figures 3, 10). Field observation during the current study allowed a more accurate description of the lithological composition of the ring complex as extrusive rocks (e.g. foliated basalts, blocky basalts, red basalts, and trachytic basalts). Intrusive rocks (e.g., Nepheline syenite, syenite, alkaline granites) (Figure 8c). The overlap of brownish kaolinitic sandstone units on the ring complex is strong evidence that the ring complex precedes all cretaceous sedimentary units (Figure 8b).

The mapping project EGPC-Conoco Coral [16] generated a geological map at 1:500,000, including the study area. This map classified the sedimentary cover into three geological units and represented the structural features as lineaments. The multispectral images of Landsat 8 enabled a more accurate distribution of the sedimentary units (Figures 3, 10) and the lithological composition of each unit was verified during the field trip (Figure 8). The high-resolution imagery dataset allowed detailed identification of structural architecture of the study area (Figures 6, 10).

Is a geological mapping project at 1:100,000. This project defined three geological formations to occupy the study area (Abu Hagga, Timsah and Umm Barmil formations). Wadi alluvium and gravel fill are the Quaternary deposits defined by this project. The interpretation of multi-spectral [20].

Landsat 8 dataset shows the different distribution of lithological units defined in the current study. The new distribution of lithological units was validated through field observation.

Studied the petroleum system of Komombo, Nuqra, and Kharit. As a part of this approach, a regional surface structural map including differentiation between Cretaceous rocks and basement rocks [19]. Defined the structural features as predominantly NW-SE normal faults, which could be inherited from the Precambrian Najd fault system [26]. The field check proved that the western basement shoulder's location and faults needed to be corrected in that work. The interpretation of high-resolution images of Google Earth coupled with field check shows the existence of other fault sets in the study area (WNW-ESE, E-W, and N-S). In addition, the strike-slip movement was recognized for some faults. Field check allowed strike and dip measurements illustration on the generated map. Folds were not previously mapped in the study area. Our geo-structural map provides an integrated view of the study area's structural architecture and lithology (Figure 11).

The Basement complex is overlain by Lower Upper Cretaceous sedimentary succession consisting of three fluvial-lacustrine, coarse to very fine-grained siliciclastic lithological units: SS1, SS2, and Sh units. SS1 is a brownish kaolinitic sandstone (SS1) that unconformably overlain the basement rocks. The brownish kaolinitic sandstone unit (SS1) exposes in the southwestern and northeastern margins of the Kharit basin; the brownish kaolinitic sandstone unit (SS1) unit is overlain by the ferruginous sandstone unit (SS2). The SS2 unit comprises ferruginous fine to medium-grained sandstone. Its distribution is restricted to specific topographic highs in the study area's southeastern and northwestern parts. Multiple fine-grained lithologies (Marly shale, shale, shale with plant remains, black shale) form the Sh unit, which overlain the ferruginous sandstone unit (SS2) unit. The shale unit (Sh) covers most low-relief exposures (Figure 11).

The Igneous intrusions in the study area are ring complexes. These ring complexes occur along

the rift border zones. They intruded the Precambrian metasediments and underlay the brownish kaolinitic sandstone unit (SS1). The ring complexes in the Kharit basin consist of extrusive rocks (e.g., foliated basalts, blocky basalts, red basalts, and trachytic basalts) and intrusive rocks (e.g. Nepheline syenite, syenite, alkaline granites) (Figure 8).

The Quaternary deposits consist of alluvial, colluvial, and aeolian unconsolidated, mostly sand-sized clastics. Alluvial and colluvial deposits in the Kharit basin are concentrated in long NW to NNW oriented wadis and the associated fans or tributaries traversing the study area (e.g. Wadi Kharit, Wadi Garara, and Wadi Timsah). These wadis are of depositional origin, formed mainly because flash floods affected the study area. The aeolian deposits in the Kharit basin are predominately accumulated to form the dunes field in the southernmost part of the Kharit basin (Figure 11).

6. Conclusions

Geo-structural mapping of the Kharit basin is essential to understand its structural architecture and tectonic evolution. The current map illustrates the main structural framework and stratigraphic succession of the Kharit basin that could be the core of the future geological research about this remote and tiff region and support the ongoing hydrocarbon and mineral exploration. The utilization of false color composite (FCC) of processed satellite images incorporates with the ground truth solved the ambiguity of lithology differentiation and updated the geological units composing different exposures outcrops in the study area. The area of the Kharit basin appears as an elongated NW-oriented trough filled by Cretaceous sediments and bounded from East, West, and South by Precambrian basement rocks. The eastern and western rift boundary faults show a zigzag fault pattern encompassing two NW and WNW-oriented fault segments. Internally, the Kharit basin is subdivided into minor NW-oriented interabasinal highs and troughs. The internal troughs are filled by thick Early to Late Cretaceous continental to shallow marine sedimentary sequences.

The complex mapped fault pattern includes four trends: NW-SE, WNW-ESE, E-W, and N-S. The first two trends are the main trough bounding faults and show the vertical sense of movement, while the other two are linked fault segments and show an oblique sense of movement. In addition, several NW to WNW oriented anticlines and synclines were developed as normal drag along the footwall and hanging wall of the primary bounding fault system. Finally, it could be mentioned that the Precambrian host Kharit basin was affected mainly by the inherited Najd fault system of the late Precambrian rift-related transform system.

Acknowledgments

The authors thank GANOPE for providing subsurface data (Seismic and Well data). Earth Explorer has supported this research by providing accessibility to Landsat-8. In addition, we would like to acknowledge Dr Lamees (Quality Standard Company) for her supportive reviews that significantly improved the manuscript and Eng—Ahmed Aly for support and troubleshooting related to ENVI and ArcGIS software. The authors are also grateful to the reviewers and editorial board.

References

[1]. Stern, R. J. (1985). The Najd fault system, Saudi Arabia and Egypt: A late Precambrian rift-related transform system?. Tectonics, 4(5), 497-511.

[2]. Sultan, M., Arvidson, R. E., & Sturchio, N. C. (1986). Mapping of serpentinites in the Eastern Desert of Egypt by using Landsat thematic mapper data. *Geology*, *14*(12), 995-999.

[3]. Zoheir, B., & Lehmann, B. (2011). Listvenite–lode association at the Barramiya gold mine, Eastern Desert, Egypt. *Ore Geology Reviews*, *39*(1-2), 101-115.

[4]. Ali, K. (2013). Geophysical Studies on Wadi Hodein Basin. PhD. Faculty of Science, Al-Azhar University, Cairo, Egypt, 203 p.

[5]. Aboelkhair, H., Abdelhalim, A., Hamimi, Z., & Al-Gabali, M. (2020). Reliability of using ASTER data in lithologic mapping and alteration mineral detection of the basement complex of West Berenice, Southeastern Desert, Egypt. *Arabian Journal of Geosciences*, *13*, 1-20.

[6]. Abdelhalim, A., Aboelkhair, H., Hamimi, Z., & Al-Gabali, M. (2020). Mapping lineament features using GIS approaches: case study of Neoproterozoic basement rocks in the South-Eastern Desert of Egypt. *Arabian Journal of Geosciences*, *13*, 1-14.

[7]. Gobashy, M. M., Eldougdoug, A., Abdelazeem, M., & Abdelhalim, A. (2021). Future development of gold mineralization utilizing integrated geology and aeromagnetic techniques: A case study in the Barramiya Mining District, Central Eastern Desert of Egypt. *Natural Resources Research*, *30*, 2007-2028.

[8]. Abdeen, M. M., Ramadan, F. S., Nabawy, B. S., & El Saadawy, O. (2021). Subsurface structural setting and hydrocarbon potentiality of the Komombo and

Nuqra Basins, South Egypt: a seismic and petrophysical integrated study. *Natural Resources Research*, *30*(5), 3575-3603.

[9]. Gobashy, M. M., Abbas, E. A. S., Soliman, K. S., & Abdelhalim, A. (2022). Mapping of gold mineralization using an integrated interpretation of geological and geophysical data—A case study from West Baranes, South Eastern Desert, Egypt. *Arabian Journal of Geosciences*, *15*(22), 1692.

[10]. Ali, M., Ali, M. Y., Abdelhady, A., & Fairhead, J. D. (2022). Tectonic evolution and subsidence history of the Cretaceous basins in southern Egypt: The Komombo Basin. *Basin Research*, *34*(5), 1731-1762.

[11]. Mahmoud, Deemah Saad, Ahmed Ali Madani, Said Mohamed Said, Mohamed Mokhtar Yehia, and Tamer Nassar. 2023. "Change Detection of Surface Water of Atfih Spring by Integrated Effect of Rainfall Storms and Geological Structures Using Landsat Data." *Journal of Mining and Environment* 14 (1): 79–96. https://doi.org/10.22044/jme.2023.12516.2272.

[12]. Eldougdoug, A., Abdelazeem, M., Gobashy, M., Abdelwahed, M., Abd El-Rahman, Y., Abdelhalim, A., & Said, S. (2023). Exploring gold mineralization in altered ultramafic rocks in south Abu Marawat, Eastern Desert, Egypt. *Scientific Reports*, *13*(1), 7293.

[13]. El Gammal, E. S. A., Salem, S. M., & Greiling Reinhard, O. (2013). Geology, Morphotectonics And Geophysical Interpretation Of Wadi Garara Graben, East Aswan Egypt, Using Landsat Images. *Australian Journal of Basic and Applied Sciences*, *7*(1), 263-277.

[14]. Gobashy, M. M., Eldougdoug, A., Abdelwahed, M., Abdelazeem, M., Abd El-Rahman, Y., Abdelhalim, A., & Said, S. (2023). Role of Integrated Magnetics and Geology in Tracking and Exploring Complex Structures Controlling Gold Mineralization. Example from the Fawakheir-Atalla Gold Prospects, Eastern Desert, Egypt. *Pure and Applied Geophysics*, 1-31.

[15]. Hammad, M. A. (1975). Geological map of Egypt. *Appendix 1. Soil Survey Papers no. 11*.

[16]. Egyptian Geological Survey and Mining Authority (EGSMA), (1981), Baranis Quadrangle map, scale 1:250000

[17]. Egyptian General Petroleum Corporation-Conoco Coral, 1987. Geological map of Egypt, Scale (1:500,000). Cairo, Egypt.

[18]. Egyptian Geological Survey and Mining Authority (EGSMA), 1996, Geological map of Egypt, scale (1:100,000). Cairo.

[19]. Mostafa, A., Sehim, A., & Farouk, O. (2016). Hydrocarbon assessments of interior Cretaceous rift basins, upper Egypt. In *The proceeding 8th Mediterranean Offshore Conference (MOC), Alexandria, Egypt*.

[20]. Abdeen, M. M., Ramadan, F. S., Nabawy, B. S., & El Saadawy, O. (2021). Subsurface structural setting and hydrocarbon potentiality of the Komombo and Nuqra Basins, South Egypt: a seismic and petrophysical integrated study. *Natural Resources Research*, *30*(5), 3575-3603.

[21]. Stern, R. J., Gottfried, D., & Hedge, C. E. (1984). Late Precambrian rifting and crustal evolution in the Northeastern Desert of Egypt. *Geology*, *12*(3), 168-172.

[22]. Shackleton, R. M. (1986). Precambrian collision tectonics in Africa. *Geological Society, London, Special Publications*, *19*(1), 329-349.

[23]. El-Bialy, M. Z. (2020). Precambrian basement complex of Egypt. The geology of Egypt, 37-79.

[24]. Greiling, R. O., Abdeen, M. M., Dardir, A. A., El Akhal, H., El Ramly, M. F., El Din Kamal, G. M., ... & Sadek, M. F. (1994). A structural synthesis of the Proterozoic Arabian-Nubian Shield in Egypt. *Geologische Rundschau*, *83*, 484-501.

[25]. Dolson, J. C., Shann, M. V., Hammouda, H. A. S. S. E. I. N., Rashed, R. A. S. H. E. D., & Matbouly, S. A. Y. E. D. (1999). The petroleum potential of Egypt. *AAPG Bulletin*, *83*(12).

[26]. Said, S. M., & Sakran, S. (2020). Structural analysis and tectonic evolution of the Komombo basin, south Egypt; an example of interior Cretaceous rift. *Journal of African Earth Sciences*, *162*, 103719.

[27]. Said, S. (2013, June). The Influence of the Late Cretaceous–Early Tertiary Fold Structures on the Geometry and Evolution of Extensional Fault. In *75th EAGE Conference & Exhibition incorporating SPE EUROPEC 2013* (pp. cp-348). European Association of Geoscientists & Engineers.

[28]. Ibrahim, S., Massironi, M., Zampieri, D., Sakran, S., & Ninfo, A. (2016, May). Strike-slip Structure and Kinematics of the Nubian Faults, South Egypt. In *78th EAGE Conference and Exhibition 2016* (Vol. 2016, No. 1, pp. 1-3). European Association of Geoscientists & Engineers.

[29]. Sakran, S., & Said, S. M. (2018). Structural setting and kinematics of Nubian fault system, SE Western Desert, Egypt: An example of multi-reactivated intraplate strike-slip faults. *Journal of Structural Geology*, *107*, 93-108.

[30]. Said, S. M., & Sakran, S. (2022). Geometry and kinematics of right-lateral transpressional faults and growth folds, the western side of the Gulf of Suez, Egypt. *Geological Journal*, *57*(1), 276-291.

[31]. Kaufman, Y. J., Wald, A. E., Remer, L. A., Gao, B. C., Li, R. R., & Flynn, L. (1997). The MODIS 2.1-/spl mu/m channel-correlation with visible reflectance for use in remote sensing of aerosol. *IEEE transactions on Geoscience and Remote Sensing*, *35*(5), 1286-1298.

[32]. Matthew, M. W., Adler-Golden, S. M., Berk, A., Richtsmeier, S. C., Levine, R. Y., Bernstein, L. S., ... & Miller, D. P. (2000, August). Status of atmospheric correction using a MODTRAN4-based algorithm. In *Algorithms for multispectral, hyperspectral, and ultraspectral imagery VI* (Vol. 4049, pp. 199-207). SPIE.

[33]. El-Meselhy, A., Abdelhalim, A., & Nabawy, B. S. (2020). Geospatial analysis in groundwater resources management as a tool for reclamation areas of New Valley (El-Oweinat), Egypt. *Journal of African Earth Sciences*, *162*, 103720.

[34]. Roy, S. S., & Singh, C. K. (2018). Evaluation of spectral mapping methods of mineral aggregates and rocks along the thrust zones of Uttarakhand using hyperion data. In *Geospatial Applications for Natural Resources Management* (pp. 251-274). CRC Press.

[35]. Laben, C. A., & Brower, B. V. (2000). *U.S. Patent No. 6,011,875*. Washington, DC: U.S. Patent and Trademark Office.

[36]. Salem, S. M., & El Gammal, E. A. (2015). Iron ore prospection East Aswan, Egypt, using remote sensing techniques. *The Egyptian Journal of Remote Sensing and Space Science*, *18*(2), 195-206.

[37]. Amusuk, D. J., Hashim, M., Pour, A. B., & Musa, S. I. (2016). Utilization of landsat-8 data for lithological mapping of basement rocks of plateau state north central nigeria. *The International Archives of the Photogrammetry, Remote Sensing and Spatial Information Sciences*, *42*, 335-337.

[38]. Harrisgeospatial (2018). The Many Band Combinations of Landsat 8. [online] Available at: http://www.harrisgeospatial.com/Support/SelfHelpTools/HelpArticles/HelpArticles-Detail/TabId/2718/ArtMID/10220/ArticleID/15691/The-Many-Band-Combinations-of-Landsat-8.aspx. https://doi.org/10.1007/s11053-021-09824-6.

[39]. Sayed, F., Hammed, M. S. H., Shided, A. G., & Hussein, A. W. (2023). Implementation of Remote Sensing Techniques in Structural and Lithological Mapping of Northwestern Margin of Red Sea, Egypt. *Journal of Mining and Environment*, *14*(2), 389-411.

[40]. Liu, J.G., and Mason, P.J., (2013). Essential image processing and GIS for remote sensing. John Wiley & Sons.

[41]. CCMEO "Canada Centre for Mapping and Earth Observation", 2013. Image Classification and Analysis. [online] Available at: https://www.nrcan.gc.ca/maps-tools-publications/satellite-imagery-air-photos/remote-sensing-tutorials/image-interpretation-analysis/image-classification-and-analysis/9361.

[42]. Rajendran, S. (Ed.). (2009). *Hyperspectral remote sensing and spectral signature applications*. New India Publishing.

[43]. CCMEO "Canada Centre for Mapping and Earth Observation", 2015. Elements of Visual Interpretation. [online] Available at: https://www.nrcan.gc.ca/maps-tools-publications/satellite-imagery-air-photos/remote-sensing-tutorials/image-interpretation-analysis/elements-visual-interpretation/9291.

پیاده‌سازی داده‌های نوری و بررسی میدانی فضایی برای نقشه‌برداری ژئوساختاری حوضه شکاف داخلی: مطالعه موردی از منطقه خاریت، صحرای جنوب شرقی، مصر

احمد عبدالحلیم[1]، اسلام ابوللا[2]، شوکی سکران[1] و سعید محمد سعید[1*]

1. گروه زمین شناسی، دانشگاه قاهره، دانشکده علوم، جیزه، مصر

2. استاندارد کیفیت فناوری اطلاعات، مصر

ارسال 2023/03/29، پذیرش 2023/08/07

* نویسنده مسئول مکاتبات: szidan@cu.edu.eg

چکیده:

حوضه خاریت یک حوضه شکاف کرتاسه داخلی است که در مجموعه زیرزمین پرکامبرین سپر عربی-نوبی میزبانی شده است. تصاویر ماهواره‌ای و داده‌های ژئوفیزیکی بالقوه قبلاً حوضه را بدون مطالعه میدانی دقیق مشخص کرده بودند. منطقه خاریت منطقه ای دورافتاده و بسیار خشک است. بنابراین، استفاده از سنجش از دور برای تکمیل فرآیند نقشه برداری ژئوساختاری آن ضروری است. مجموعه داده‌های نوری چند طیفی Landsat-8 و تصاویر با وضوح بالا از Google Earth با تحقیقات میدانی برای طبقه‌بندی واحدهای سنگ‌شناسی و تعریف ساختارها ادغام شدند. این ادغام بین تصاویر ماهواره‌ای تحلیل شده و تحقیقات میدانی منجر به یک نقشه زمین شناسی با حداقل مقیاس 1:50000 برای واحدهای سنگی سنگی و حداکثر مقیاس تا 1:7000 برای نقشه برداری ساختاری شد. این نقشه یک حوضه شکاف دراز جهت شمال غربی را نشان می‌دهد که توسط یک رسوب ضخیم از توالی‌های کرتاسه پر شده است که از شرق، غرب و جنوب توسط سنگ‌های آذرین و دگرگونی پروتروزوییک محدود شده‌اند. علاوه بر این، سنگ‌های آتشفشانی مربوط به شکاف در امتداد سیستم گسل مرزی غربی حوضه نقشه برداری شدند. گسل‌های اصلی نقشه‌برداری شده در سه روند NW-SE، WNW-ENE و N-S ترسیم شدند، در حالی که چندین چین جهت NW به عنوان یک کشش معمولی از گسل‌های مرزی اصلی ایجاد می‌شوند. گسترش کرتاسه اولیه در امتداد خطواره‌های پرکامبرین به ارث رسیده این الگوی گسلی و چین های مرتبط با آن را منتشر کرد. این عناصر ساختاری معماری منطقه مورد مطالعه را به صورت چند گرابن با توالی کرتاسه ضخیم پیکربندی کردند.

کلمات کلیدی: نقشه برداری ژئوساختاری، حوضه خاریت، Landsat-8، ساختار شکافی، تکتونیک کرتاسه.